To be presented at IEEE EMBC 2001 in Istanbul, 25-28 October 2001.

Spatio-temporal Multi-dipole Source Localization Using ICA and Lead-Fields in FEM Head Models

Leonid Zhukov[1], David Weinstein[2], Chris Johnson[2], Rob Macleod[2]
Department of Computer Science, California Institute of Technology, Pasadena, CA, USA
Scientific Computing and Imaging Institute, University of Utah, Salt Lake City, UT, USA

Abstract— **In this paper we introduce a framework for the solution of the multi-dipole, time-dependent, source localization problem in realistic head models. Our technique combines a PCA/ICA signal decomposition with an FEM-based lead-field approach to source localization. This combination enables the efficient localization of multiple dipole sources.**

Keywords— **EEG, source localization, ICA, PCA, FEM, lead-fields**

I. Introduction

In this paper we combine and further develop the ideas first proposed in [1] and [2]: we present an efficient technique for performing multi-dipole source localization in a realistic head model on time-dependent data. The first part of our algorithm considers just the geometry of the problem, building a finite element method (FEM) lead-field matrix for the head model that projects all possible source configurations onto electrodes. The second part applies principal component analysis (PCA) and independent component analysis (ICA) to the temporal electroencephalography (EEG) data, finding the signal subspace of the data and the mixing matrix for statistically independent sources. Finally, we use the lead-field and mixing matrices to spatially localize all contributing sources via an exhaustive search or standard optimization method.

The major assumptions used in this paper are that the dipole source are independent and stationary. That is, every source is fixed in space, and has an activation pattern that is independent from all other dipoles. The number of active dipoles is assumed to be less than the number of recording channels.

II. FEM Lead-Fields

The lead-field matrix, $\mathbf{L}$, defines a projection from current sources at discrete locations in the cranium to potential measurements at discrete recording sites on the scalp and is depicted graphically in Fig (1). Every entry $\bar{L}_{ij} \equiv (L^x_{ij}, L^y_{ij}, L^z_{ij})$ of the matrix corresponds to the potential that would be measured at recording site ϕ_i due specifically to dipole source $\bar{p}_j$ with components (p^x_j, p^y_j, p^z_j):

$$\phi_i = \bar{L}_{ij}\bar{p}_j = L^x_{ij}p^x_j + L^y_{ij}p^y_j + L^z_{ij}p^z_j. \qquad (1)$$

Then a column $\bar{\mathbf{L}}_j \equiv [\bar{L}_{1,j}, \bar{L}_{2,j}, .., \bar{L}_{N,j}]^T$ of the lead-field matrix projects a source $\bar{p}_j$ in the element j onto all of the electrodes:

$$\boldsymbol{\phi} = \bar{\mathbf{L}}_j\bar{p}_j. \qquad (2)$$

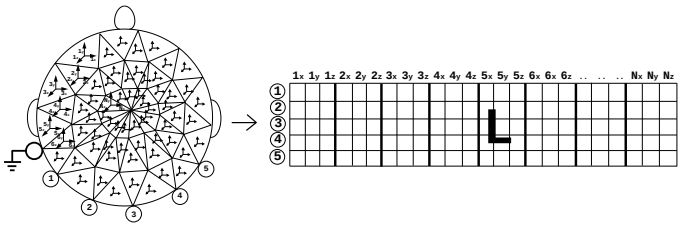

Fig. 1. Depiction of the lead-field matrix. The dipole in each element corresponds to a major column of $\mathbf{L}$, each electrode corresponds to a row of $\mathbf{L}$, and each entry of $\mathbf{L}$ corresponds to the potential measured at a particular electrode due to a particular source.

With the lead-field approach, sources are generally located in *every* element of the mesh covering the domain of interest and form the source vector $\bar{\mathbf{p}}$. Electrode potentials are the linear combinations of those sources with weights provided from the lead-field matrix. When considering time dependencies, the three dipole components are assigned the same time activation $s_j(t_k)$. The lead-field matrix does not depend on time, and the vector of electrode potentials is then given by:

$$\boldsymbol{\phi}(t_k) = \sum_j \bar{\mathbf{L}}_j\bar{\mathbf{p}}_j s_j(t). \qquad (3)$$

Detailed descriptions of different possible lead-field matrices and efficient ways of computing them for FEM models can be found in [1].

III. Statistical Processing - PCA and ICA

For a given electrode configuration, the time-dependent data can be arranged as a matrix, where columns correspond to time and rows correspond to channels (electrodes) $\Phi = \boldsymbol{\phi}(t_k)$.

Below, we follow the procedure described in [2]. We begin by applying PCA (SVD) decomposition to the covariance matrix of the data $R = \Phi\Phi'$ and constructing the signal and noise subspaces spanned by the eigenvectors of the covariance matrix. The signal subspace will consist of the singular vectors with singular values greater than a chosen noise threshold, and the noise subspace will be composed of the remaining eigenvectors [3].

$$\mathbf{R} = \mathbf{U}\cdot\boldsymbol{\Lambda}\cdot\mathbf{U}^T = \mathbf{U}_s\cdot\boldsymbol{\Lambda}_s\cdot\mathbf{U}_s^T + \mathbf{U}_n\cdot\boldsymbol{\Lambda}_n\cdot\mathbf{U}_n^T. \qquad (4)$$

The projection of the original data onto the signal subspace

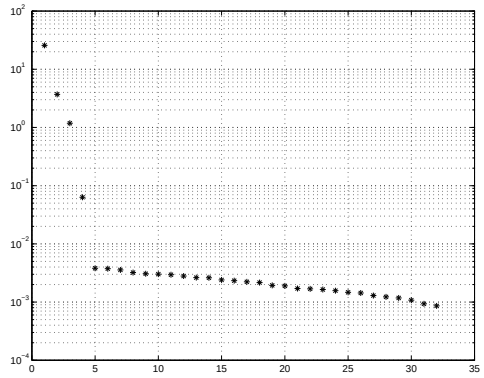

Fig. 2. First 32 singular values of the covariance matrix. Only the first three singular values contribute to the signal subspace, with the rest constituting the noise subspace.

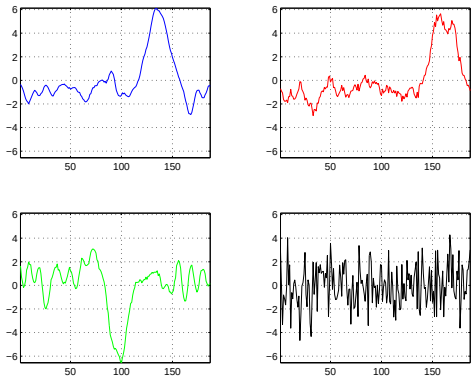

Fig. 3. ICA activation maps obtained by unmixing the signals from the signal subspace.

is given by:

$$\boldsymbol{\phi}_s(t_k) = \sqrt{\boldsymbol{\Lambda}_s}^{(-1)} \cdot \mathbf{U}_s^T \cdot \boldsymbol{\phi}(t_k), \tag{5}$$

where $\boldsymbol{\Lambda}_s$ and $\mathbf{U}_s$ are the signal subspace singular values and singular vectors, respectively.

Next, we apply the ICA algorithm to decompose the signal subspace into independent components. That is, we find an "unmixing" matrix $\mathbf{W}$, such that:

$$\mathbf{W} \cdot \phi_s(t_k) = s(t_k), \tag{6}$$

with $E\{s_i^m(t_k)s_j^n(t_k)\} = 0$ for all values m and n. There exist several algorithms for ICA decompositions. We use the infomax algorithm [4], which is based on minimization of mutual information between channels.

Combining the two previous equations, Eq (5) and Eq (6), we construct the projection matrix

$$\mathbf{M} = \mathbf{U}_s \cdot \sqrt{\boldsymbol{\Lambda}_\mathbf{s}} \cdot \mathbf{W}^{(-1)}, \tag{7}$$

such that

$$\boldsymbol{\phi}(t_k) = \mathbf{M}\mathbf{s}(t_k). \tag{8}$$

IV. Algorithm

Comparing Eq (3) and Eq (8) we note that though matrices $\mathbf{L}$ and $\mathbf{M}$ were derived from separate analyses of the geometric data and the temporal channel data, they both describe the projection of sources onto electrode recordings. Specifically, $\mathbf{L}$ describes the signature that a single dipole leaves when projected onto the electrodes, and $\mathbf{M}$ defines how a collection of independent signatures are mixed to produce the recorded channel data. Looking at the shape of the matrices, we note that the computed matrix $\mathbf{M}$ has dimensionality $N_{elec} \times N_{source}$, as it provides mixing columns only for *existing sources*. In contrast, matrix $\mathbf{L}$ describes the projection of all possible sources in every element onto the electrodes, and thus has a dimensionality of $N_{elec} \times N_{elem}$. Then for every separate "source" column of $\mathbf{M}$, we search for the column from $\bar{\mathbf{L}}$ (and corresponding dipole components $\bar{p}$) that can best reproduce that source in the least squares sense. In linear FEM, all positions of the dipole within an element are equivalent, so the dipole location is fully specified by an element (column) index j. We perform a minimization of the misfit function

$$C_k(j, \bar{p}_j) = ||\mathbf{M}_k - p_j^x \mathbf{L}_j^x - p_j^y \mathbf{L}_j^y - p_j^z \mathbf{L}_j^z||_2. \tag{9}$$

with respect to a discrete j and a continuous p_j, under the constraint that there exists only a single nonzero entry $\hat{\bar{p}}_j \equiv (p_j^x, p_j^y, p_j^z)$ in the solution vector $\bar{\mathbf{p}}$; that is, our source is a single dipole. Since measured potentials are linear combinations of dipole components (see Eq (1)), we can split the minimization problem into two parts and use a closed form, least squares solution for the dipole orientation:

$$\hat{\bar{p}}_j = (\bar{\mathbf{L}}_j^T \bar{\mathbf{L}}_j)^{-1} \bar{\mathbf{L}}_j^T \mathbf{M}_k. \tag{10}$$

Then the misfit function will explicitly depend only on the location j:

$$C_k(j) = ||\mathbf{M}_k - \bar{\mathbf{L}}_j \hat{\bar{p}}_j||_2. \tag{11}$$

To find the global minimum of the discrete function $C_k(j)$, we can use either an exhaustive search over all columns of $\mathbf{L}$ or an advanced optimization algorithm, such as multi-start downhill simplex [5] or simulated annealing [6].

The described minimization procedure is then repeated for all columns of matrix $\mathbf{M}_k$, thus recovering the location and orientation of all sources one at a time.

V. Numerical Simulations

We constructed a realistic finite element head model from a volume MRI scan. The MRI data was segmented at the Brigham and Women's hospital [7], and a mesh was constructed using Krysl's variational Delaunay algorithm [8]. The full mesh contained 396,000 elements and 70,000 nodes. We then coregistered 129 digitized electrode locations with the MR scalp surface.

In order to simulate time-dependent recordings, we first computed a forward solution due to each of three simulated epileptic sources, assuming dipoles of unit-strength. Each source produced a *signature* of values at the simulated electrode sites. To extend the single-instant values at the electrodes into time-dependent signals, we scaled

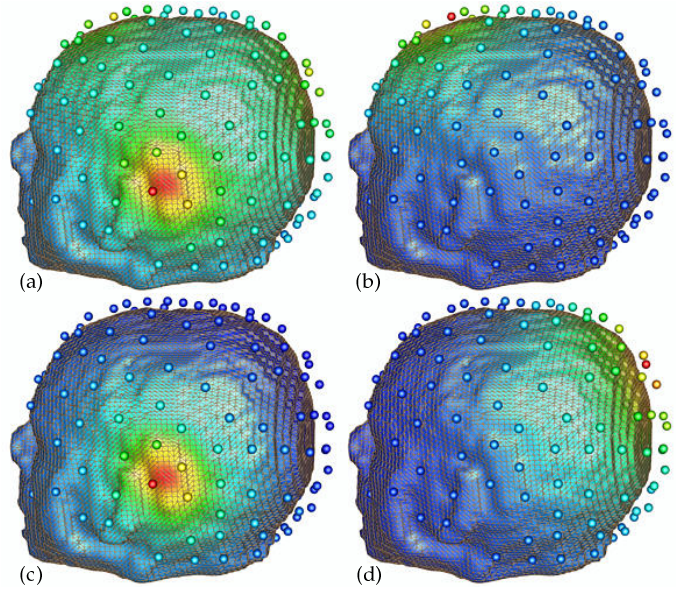

Fig. 4. Activation maps for a single instant in time. Electrode potentials have been interpolated across the scalp surface of our finite element mesh for visualization purposes. The original "measured" activation is shown in (a); the statistically separated activation maps are shown in (b)-(d).

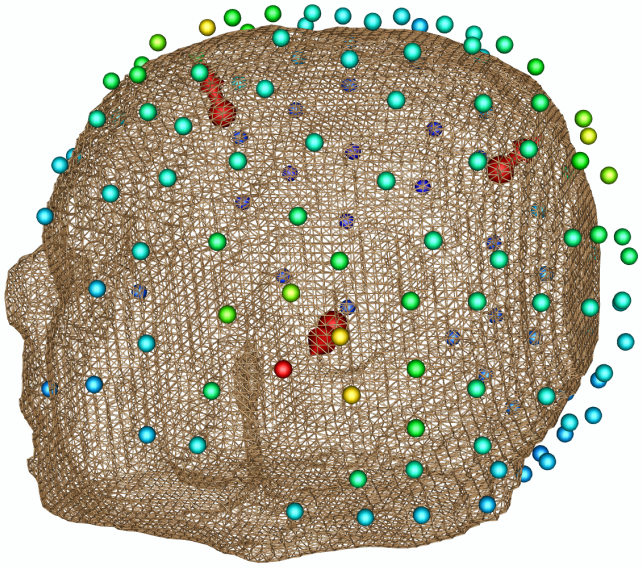

Fig. 5. Recovered dipole positions. One source was localized for each of the activation maps in Fig (4b-d). Two of the three sources were recovered exactly; the third was localized within 3 mm of its true location.

the values of each signature by pre-recorded clinical activation signals. Finally, we added the three simulated time courses together, along with 2% noise to simulate physical EEG measurements.

Then we followed the algorithm outlined above in order to recover the original source locations and orientations. We started by building $\mathbf{L}$ using the reciprocity method of Weinstein *et al* [1]. We chose one electrode to be a current sink, and for each of the remaining electrodes, we placed a current source at that electrode and solved a forward simulation. Each simulation computed the electric field at each element in our model, which we then stored as a row of $\mathbf{L}$. Each solution required on average 8 seconds of wall-clock time using 8 SGI MIPS R10000 processors. For the 128 pairings, this totaled 18 minutes to compute all of $\mathbf{L}$.

We then performed PCA on the EEG time-dependent data and obtained the singular values shown in Fig (2). Analyzing the singular values, we made the conservative deduction that the signal subspace consisted of the first four singular vectors. Working with the contribution of these four components, we performed ICA, resulting in the mixing matrix and activation maps shown in Fig (3). (Notice that there are, in fact, only three signal components; the fourth component is clearly noise.)

Finally, we used both the multi-restart simplex search [5] and the simulated annealing [6] algorithms to find the global minimum of the misfit function. Both algorithms recovered the same source dipoles. The simplex search algorithm was restarted eight times for each source in order to improve the likelihood that we had localized the global minimum. We validated our recovered minima through an exhaustive search of the domain. Due to the 2% error that we added to the original signal, the misfit function for the recovered sources was not equal to zero. For two of the three sources, the optimal misfits were 0.0002 and 0.0009 (misfit $= 1 - ||$correlation coefficient$||$) . For the third source, the optimal misfit was 0.053, and was actually localized one element (3 mm) away from the true source location.

The summed activation maps are shown in Fig (4a), and the recovered independent activations are shown in Fig (4b-d). The positions of the recovered dipole sources are shown in Fig (5).

VI. Acknowledgments

This work was supported by the National Institutes of Health, National Center for Research Resources, grant number 1-P41-RR12553-2.

References

[1] Weinstein D, Zhukov L, Johnson C. *Lead-field bases for electroencephalography source imaging*, Ann. Biomed. Eng., 28:1-7,2000.

[2] Zhukov L, Weinstein D, Johnson C. *Independent component analysis for EEG source localization*, IEEE Eng. Med. Biol. Mag., 19(3):87-96,2000.

[3] Mosher JC, Lewis PS, Leahy RM. *Multiple dipole modeling and localization from spatio-temporal MEG data*, IEEE Trans. Biomed. Eng. 39: 541-57, 1992.

[4] Makeig S, Bell AJ, Jung T-P, Sejnowski TJ. *Independent Component Analysis of Electroencephalographic data*, Advances in Neural Information Processing Systems 8:145-151, 1996.

[5] Nedler JA, Mead R. *A simplex method for function minimization*, Comput. J. (UK) 7:308-313, 1965.

[6] Metropolis N, Rosenbluth A, Rosenbluth R, Teller A, Teller E. *Equation of state calculations by fast computing machines*, J. Chem. Phys. 21:1087-1092, 1953.

[7] Wells WM, Grimson WEL, Kikinis R, Jolesz FA. *Statistical intensity correction and segmentation of MRI data*, Visualization in Biomedical Computing 13-24, 1994.

[8] Krysl P, Oritz M. *Variational Delaunay Approach to the Generation of Tetrahedral Finite Element Meshes*, Int. J. Numer. Methods Eng. (in press).